

This material is posted here with permission of the IEEE. Such permission of the IEEE does not in any way imply IEEE endorsement of any of Helsinki University of Technology's products or services. Internal or personal use of this material is permitted. However, permission to reprint/republish this material for advertising or promotional purposes or for creating new collective works for resale or redistribution must be obtained from the IEEE by writing to [pubs-permissions@ieee.org](mailto:pubs-permissions@ieee.org).

By choosing to view this document, you agree to all provisions of the copyright laws protecting it.

# Microreplicated RF Toroidal Inductor

Vladimir Ermolov, Tomas Lindström, Heikki Nieminen, Mikael Olsson, Michael Read, Tapani Ryhänen, Samuli Silanto, and Simon Uhrberg

**Abstract**—This paper reports on the modeling and fabrication of a truly three-dimensional high-quality-factor toroidal inductor using polymer replication processes. The critical dimensions are in the micrometer range, and the applied manufacturing method is based on polymer replication. Electrical measurements show that the inductor with an inductance of 6.0 nH exhibits a peak quality factor of 50 at a frequency of 3 GHz. Model verified by the measurement results shows that further improvement is still possible. Furthermore, the applied manufacturing technique can be extended to become a flexible packaging platform.

**Index Terms**—Inductors, micromachining, plastics, RF microelectromechanical system (MEMS), transformer.

## I. INTRODUCTION

THERE IS AN increasing need for high-performance low-cost inductors in the telecommunication industry. High-performance RF inductors are key components for implementing low-noise RF voltage-controlled oscillators, low-loss impedance matching circuits, low-loss passive filters, and inductive loads. Critical parameters of an inductor include inductance value, quality ( $Q$ ) factor, and self-resonance frequency.

For inductors, the fabrication method is normally either thin-film processing or wire winding [1]–[3]. Thin-film spiral inductors use integrated-circuit (IC) technology and are more easily miniaturized and integrated than wire wound inductors. However, spiral inductors implemented by silicon micromachining processes suffer from several power-dissipation mechanisms, leading to a poor inductor  $Q$ . The mechanisms that reduce the  $Q$  include losses from coil resistance, losses from eddy currents circulating below the spiral in the silicon substrate, and self-resonance of the coil. In order to increase the  $Q$  of the spiral inductor, several approaches have been reported, e.g., having a thick metallization or multilayer metallization [4], [5], a patterned ground shield below the inductor [6], a thick dielectric layer to separate the spiral from the substrate [7], using high-resistivity ( $>4$  k $\Omega$ ) silicon [4], or fabricating a suspended inductor by etching the substrate underneath [8], [9].

Recently, three-dimensional (3-D) on-chip inductors have been proposed as an alternative solution for high-performance inductors. These inductors have been made using 3-D laser lithography [10], by deformation of a sacrificial polymer under the coil [11], by the technique of self-assembled inductors

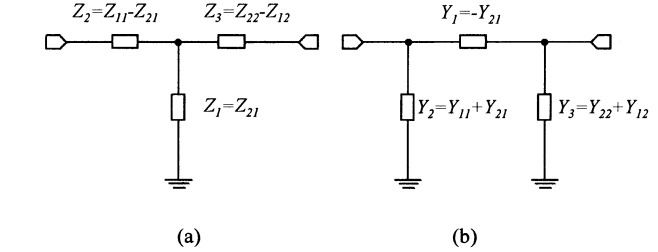


Fig. 1. (a) T-network and its relationship to the  $Z$ -parameter. (b)  $\pi$ -network and its relationship to  $Y$ -parameters.

[12], or using an ordinary IC process having several metal layers [13]. The 3-D microstructure used in these approaches minimizes the device capacitive coupling to the substrate and eddy-current loss. However, these on-chip 3-D inductors have a  $Q$  much lower than traditional bulk 3-D wire wound inductors [3].

It is well known [14] that inductors with toroidal geometry have optimal electromagnetic characteristics: higher  $Q$  compared to planar coils and lower interference with surrounding circuits, because most of the electromagnetic field is concentrated inside the torus. However, wire wound inductors are expensive and it is difficult to produce truly 3-D toroidal structures with conventional IC processes.

The aim of this paper is to report on the fabrication of a micromachined, truly 3-D inductor with toroidal geometry. The critical dimensions are in the micrometer-range and the manufacturing method is an inexpensive polymer replication process.

## II. MODEL AND DESIGN CONSIDERATIONS

### A. Definition of $Q$

The  $Q$  of an inductor can be defined in several ways [6], [15], [16]. The definitions depend very much on the intended application of the inductor. In this paper, the  $Q$  is defined as

$$Q(f) = \frac{X_m(f)}{R_m(f)} \quad (1)$$

where  $f$  is the operating frequency, and  $R_m(f)$  and  $X_m(f)$  are the real and imaginary parts of the inductor impedance ( $Z$ ), respectively. The inductor impedance can be calculated from measured  $S$ -parameters, for instance, using a T- or  $\pi$ -network, as shown in Fig. 1. Since the inductance is on the path between input and output ports, this yields two equations for the inductor impedance as follows:

$$Z = Z_{11} + Z_{22} - Z_{21} - Z_{12} \quad (2)$$

or

$$Z = -\frac{1}{Y_{21}}. \quad (3)$$

Manuscript received January 21, 2003; revised May 28, 2003. This work was supported by the Finnish National Technology Agency.

V. Ermolov, H. Nieminen, T. Ryhänen, and S. Silanto are with the Nokia Research Center, Helsinki FIN-00045, Finland (e-mail: vladimir.ermolov@nokia.com).

T. Lindström, M. Olsson, M. Read, and S. Uhrberg are with Åmic AB, SE-75183 Uppsala, Sweden (e-mail: tomas.lindstrom@amic.se).

Digital Object Identifier 10.1109/TMTT.2003.821236

It should be noted that both of these two ways neglect the effect of some parasitic losses on the inductor impedance.

### B. Dependency of $Q$ on Device Parameters

The behavior of an inductor  $Q$  at frequencies below the self-resonance can be thought to be composed of three factors

$$Q \approx \frac{\omega L}{R_s(\omega)} \cdot (\text{substrate loss factor}) \cdot (\text{self-resonance factor}). \quad (4)$$

The first factor is the geometrical quality factor of the coil, where  $\omega$  depends on the frequency ( $\omega = 2\pi f$ ),  $L$  is the inductance, and  $R_s(\omega)$  is the series resistance. The substrate loss and self-resonance factor of the coil depend on the resistivity of the substrate and the parasitic capacitance of the coil, respectively. Optimization of the first term of (4) for a planar inductor on a low-loss substrate leads to linear dependence between the coil area and  $Q$  [17] as follows:

$$Q_{\text{max-2D}} \approx \frac{1}{8} D_{\text{out}} / \delta_{\text{skin}} \quad (5)$$

where  $D_{\text{out}}$  is the outer diameter of the coil, and  $\delta_{\text{skin}}$  is the skin depth. For example, a planar coil with a 1-mm<sup>2</sup> area optimally has a  $Q$  of approximately 50 at 1 GHz [12]. Similar dependency of the  $Q$  on the device geometry can also be derived for the toroidal coil. The inductance of the toroidal coil is

$$L = \frac{\mu_0 \mu_r N^2 r_{\text{torus}}^2}{2r_{\text{coil}}} \quad (6)$$

and

$$r_{\text{coil}} = \frac{D_{\text{out}}}{2} - r_{\text{torus}} \quad (7)$$

where  $N$  is the number of turns,  $r_{\text{torus}}$  is the radius of the torus cross section,  $r_{\text{coil}}$  is the radius of the coil,  $\mu_0$  is the vacuum permeability, and  $\mu_r$  is the relative magnetic permeability. The series resistance, when the thickness of the wire is much less than the width of the wire, is

$$R_s = \frac{\alpha(f) \cdot N^2 \cdot \pi \cdot r_{\text{torus}} \cdot \rho}{\delta_{\text{skin}} \cdot (2\pi r_{\text{coil}} - N \cdot s_{\text{coil}})} \quad (8)$$

where  $\alpha(f)$  is a coefficient taking into account current crowding effects,  $\rho$  is the resistivity, and  $s_{\text{coil}}$  is the separation between the turns of the coil. The current crowding effect is the tendency of the current in neighboring conductors to change the current distribution inside the conductor. This increases the series resistance. In addition, the skin effect has a well-known frequency dependency

$$\delta_{\text{skin}} = \sqrt{\frac{\rho}{\mu_0 \mu_r \cdot \pi \cdot f}}. \quad (9)$$

By combining (5)–(9), the maximum estimate for a toroidal coil  $Q$  at low frequencies can be derived as follows:

$$Q_{\text{max-3D}} = \sqrt{\frac{\mu_0 \cdot \mu_r}{\pi \cdot \rho}} \frac{\sqrt{f} \cdot r_{\text{torus}} \cdot (2 \cdot \pi \cdot r_{\text{coil}} - N \cdot s_{\text{coil}})}{\alpha(f) \cdot r_{\text{coil}}}. \quad (10)$$

As a result, the  $Q$  of the toroidal inductor is found to depend on  $r_{\text{torus}}$ . Fig. 2 shows the  $Q$  at 0.9 GHz as a function of the radius

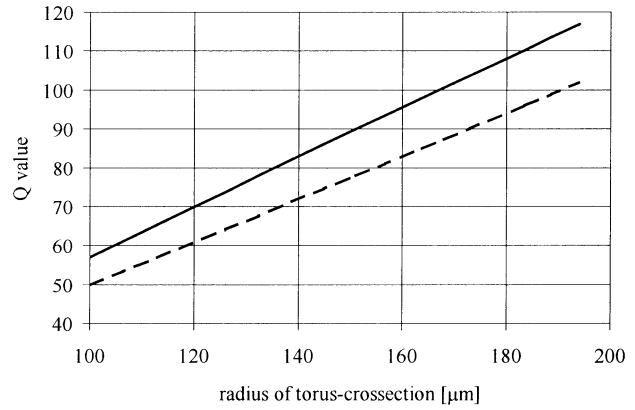


Fig. 2.  $Q$  at 0.9 GHz as a function of the radius of the torus cross section. The dashed line is the  $Q$  of an inductor made of gold and the solid line is the  $Q$  of an inductor made of copper. The dimensions of the coils are  $D_{\text{out}} = 1$  mm,  $s_{\text{coil}} = 15$   $\mu\text{m}$ , and the metal thickness is 8  $\mu\text{m}$ . The number of turns was varied to keep the inductance at 5 nH.

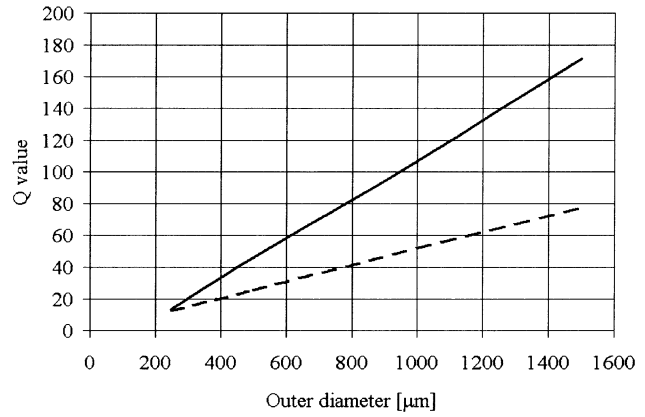


Fig. 3.  $Q$  versus the outer diameter of an optimized planar (dashed line) and toroidal (solid line) inductor at a frequency of 1 GHz. The inductance is 5 nH for both devices and the gold thickness is 8  $\mu\text{m}$ . There is ratio of 0.2 between  $2r_{\text{torus}}$  and  $D_{\text{out}}$ .

of the torus cross section. The dashed line depicts a coil made of gold ( $\rho_{\text{Au}} = 2.20 \cdot 10^{-8}$   $\Omega\cdot\text{m}$ ) and the continuous line depicts a coil made of copper ( $\rho_{\text{Cu}} = 1.67 \cdot 10^{-8}$   $\Omega \cdot \text{m}$ ). Both have dimensions  $D_{\text{out}} = 1$  mm and  $s_{\text{coil}} = 15$   $\mu\text{m}$ , and the metal thickness is 8  $\mu\text{m}$ . The number of turns was varied to keep the inductance at 5 nH.

Fig. 3 shows the  $Q$  of a toroidal and a planar coil as a function of the outer diameter. The  $Q$  of the planar coil was plotted using (5). In the case of a toroidal coil, we attempted to design a 5-nH coil with a ratio of 0.2 between  $2r_{\text{torus}}$  and  $D_{\text{out}}$ . Both coils are made of gold. The height of the conductor is 8  $\mu\text{m}$  and the frequency is 1 GHz.

It can be seen that the  $Q$  of the toroidal inductor exceeds the  $Q$  of the optimized planar coil with a similar outer diameter by approximately a factor two. For example,  $Q$  of 180 can be reached for an ideal toroidal inductor with  $D_{\text{out}} = 1.5$  mm and  $r_{\text{torus}} = 315$   $\mu\text{m}$ .

### C. Equivalent-Circuit Model of Toroidal Coil

The  $Q$  calculated using (10) does not, however, take into account parasitic losses. An equivalent-circuit model of the toroidal inductor that includes the effects of the parasitics is

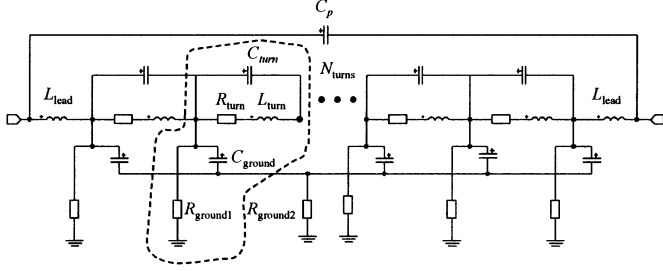


Fig. 4. Equivalent circuit of a toroidal inductor. The circuit representing one turn of the coil is inside the dashed line. The parameters are defined in the above text.

shown in Fig. 4. The model describes each turn of the coil with inductance  $L_{\text{turn}}$ , series resistance  $R_{\text{turn}}$ , capacitance  $C_{\text{turn}}$  between the adjacent turns, capacitance  $C_{\text{ground}}$  of the single coil turn to ground, substrate losses  $R_{\text{ground1}}$ , and capacitive ground path losses  $R_{\text{ground2}}$ . In addition, there is inductance  $L_{\text{lead}}$  from the leads and capacitance  $C_p$  as coupling between the first and last turns of the coil. Consequently,  $C_p$  has the same value as  $C_{\text{turn}}$ .

At high frequencies, the series resistance of the coil depends primarily on the skin depth, which limits the penetration of the field into the conductor and, secondly, on the current crowding in the coil turns. It is known that, in the case of a toroidal inductor, the current is concentrated mainly on the internal surface and at the edges of the coil turns. The series resistance of the coil at frequencies from dc to 10 GHz can be estimated by

$$R_{\text{series}} \approx R_{\text{DC}} \left[ 1 + \left( \frac{f}{f_{\text{cr}}} \right)^{\alpha_1 + \alpha_2} \right] \quad (11)$$

and

$$R_{\text{DC}} = \frac{2\pi r_{\text{torus}} N^2 \rho}{2\pi r_{\text{coil}} - N \cdot s_{\text{coil}}} \quad (12)$$

where  $R_{\text{DC}}$  is the total series resistance of the coil at dc,  $f_{\text{cr}}$  is the critical frequency, and  $\alpha_1$  and  $\alpha_2$  are the coefficients related to skin depth and current crowding, respectively. The values of  $L_{\text{turn}}$  and  $R_{\text{turn}}$  can be estimated using very simple approximations

$$L_{\text{turn}} = \frac{\mu_0 \cdot N \cdot r_{\text{torus}}^2}{2 \cdot r_{\text{coil}}} \quad (13)$$

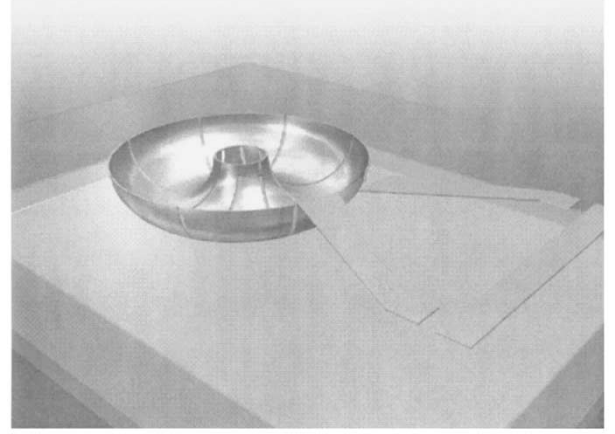
and

$$R_{\text{turn}} = \frac{R_{\text{series}}}{N}. \quad (14)$$

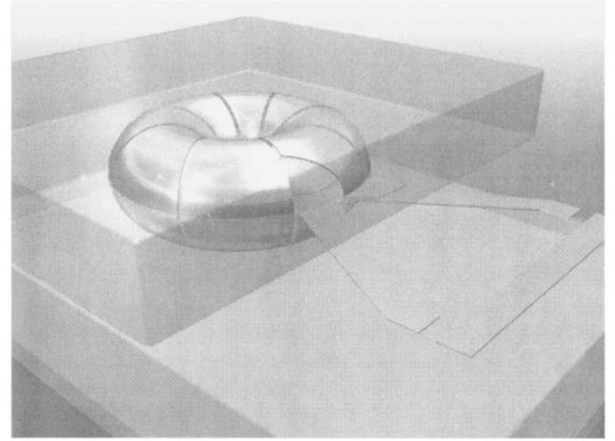
Capacitance  $C_{\text{ground}}$  is calculated from [18]

$$C_{\text{ground}} = \frac{2\pi \cdot r_{\text{coil}} \cdot \varepsilon}{59.952 \cdot N \cdot V_0 \cdot \ln \left( \frac{2 \cdot h}{D_{\text{torus}}} + \sqrt{\left( \frac{2 \cdot h}{D_{\text{torus}}} \right)^2 - 1} \right)} \quad (15)$$

where  $\varepsilon$  is the permittivity of the substrate material,  $h$  is the thickness of the substrate material,  $V_0$  is velocity of light, and  $D_{\text{torus}}$  is the diameter of the torus cross section. A numerical simulation program, i.e., QvalueC, modified for a solenoid coil, was used to calculate  $C_{\text{turn}}$  of the inductor [17]. The in-



(a)



(b)

Fig. 5. Visualization of the proposed method of fabrication. (a) Horizontal split of the toroidal inductor. (b) Joining of two halves to achieve the final geometry.

ductor model was implemented in an APLAC circuit simulator (APLAC Solutions Corporation, Espoo, Finland).

### III. DETAILS OF FABRICATION

#### A. Design of Toroidal Inductor

The chosen design of the inductor was a compromise between minimizing electrical losses due to ohmic losses, dielectric losses, and parasitic coupling, as well as obeying the restraints and limitations that are determined by the manufacturing process. In short, it was decided to fabricate a 15-turn toroidal inductor with a 20- $\mu\text{m}$  electrode separation, an inner diameter of 520  $\mu\text{m}$ , an outer diameter of 1000  $\mu\text{m}$ , and a torus diameter of 240  $\mu\text{m}$ . The electrode material can be chosen from several conductors; in this study, gold was used. The metal thickness should be thick enough to match the skin effect in the proposed frequency region, which was <8 GHz.

In order to achieve full 3-D geometry, the design was separated into two halves, as shown in Fig. 5. The idea was to fabricate each half separately and then join the two to make the final component. For this procedure to work, overlapping contact zones had to be introduced to increase the contact area between the two halves; the width of these contact zones was approximately 20  $\mu\text{m}$ .

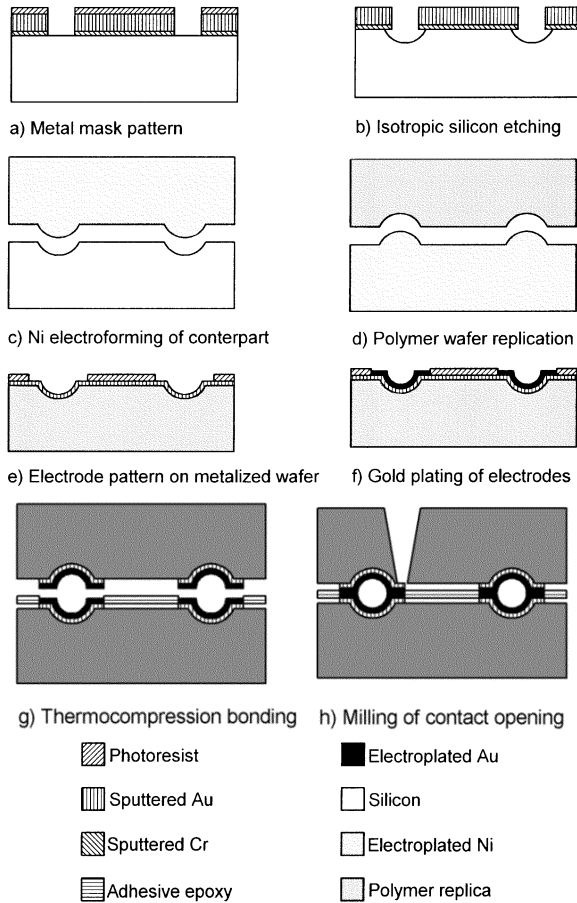
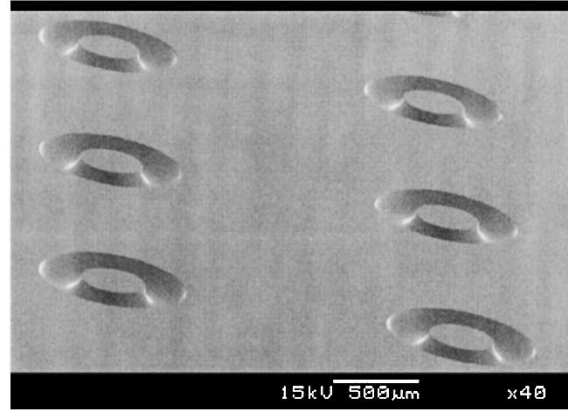


Fig. 6. Manufacturing process steps for the toroidal inductor.

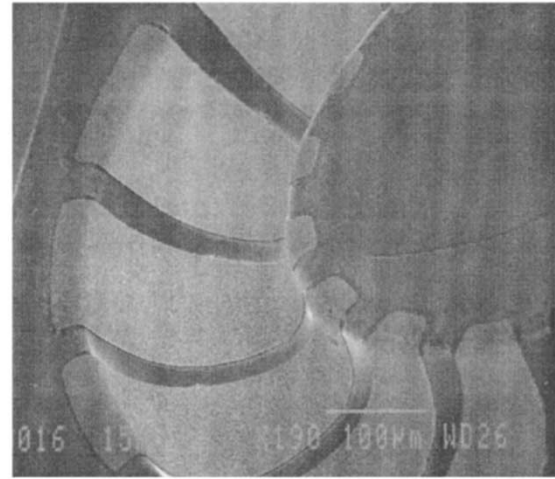
### B. Substrate Manufacturing

The idea with polymer replication is to use the accuracy and small features available, for example, in silicon micro-machining processes, in combination with the production economy from the optical data storage industry (cf. CD/DVD fabrication technology) [19], [20]. The manufacturing process steps for the toroidal inductor are illustrated in Fig. 6. Typically, a master structure is produced in silicon or glass with the desired geometry. Electroforming a negative copy of the master then creates a mould insert. Finally, polymer replicas can be produced in large quantities by using these inserts in different replication methods such as injection moulding, casting, or hot embossing [21].

Depending on the physical and chemical requirements of the final product, there is a wide range of thermoplastic and thermosetting polymer materials to choose from. In this study, we have chosen to work with injection moulded thermoplastics. The reason for this is twofold. Firstly, the dielectric properties for some of the thermoplastic polymers is superior to thermosetting materials. This is specifically the case for the cyclo-olefin polymer (COP) used in this investigation. Secondly, it is easier to obtain flat and stress-free wafers by injection moulding compared to casting with thermosetting polymers. Also, if one adds the aspect of production economy, injection moulding is to be favored.



(a)



(b)

Fig. 7. (a) Example of an isotropically etched profile in silicon. This structure was later transferred into a metallic negative by electroforming. (b) Example of a polymer substrate with gold electrodes metallized over 90° corners.

### C. Master Fabrication

The masters were produced by isotropic silicon etching [22]. In order to achieve high isotropy, it is necessary to etch without stirring and with the wafer lying horizontally and the etch features upwards. We choose to work with a 96 : 4 or 91 : 9  $\text{HNO}_3$  (69%) :  $\text{HF}$  (50%) solution. Thus, no acetic acid was used. This gives a polishing etch with smooth surfaces. In our case, we achieved an etch rate of approximately  $1 \mu\text{m}/\text{min}$  at room temperature. The final etch depth was  $120 \mu\text{m}$ . The isotropy attained, or width : depth ratio was approximately 1 : 0.96. Fig. 7(a) depicts one of the silicon masters used in this investigation.

### D. Replication Step

The silicon master structure was transferred into a  $300\text{-}\mu\text{m}$ -thick metallic counterpart by electroforming. This was achieved by plating nickel from a sulfamate electrolyte. Obviously, the obtained mould insert has the negative structure of the original. The substrates were then injection moulded in two different polymers, i.e., polycarbonate (PC) (Makrolon DP

1–1265 from Bayer Polymers, Leverkusen, Germany) and COP (Zeonex 480R from ZEON Corporation, Tokyo, Japan).

These materials exhibit different electrical properties: the dielectric constant of PC is approximately 3.5 at 1 MHz, and the loss tangent is approximately 0.01. In comparison, the COP material has a dielectric constant of 2.3 for COP and a loss tangent of 0.0002. The moulder used was a modified injection-moulding machine from the CD/DVD industry (Alpha Swden, Sundbyberg, Sweden).

#### E. Electrode Metallization

Electrode patterning can be done by various methods depending on the required accuracy. In this study, the electrodes were defined lithographically by applying a conformal photo resist layer (PEPR 2400 from the Shipley Company, Marlborough, MA) onto the polymer substrates. After resist development, electronic-quality pure gold was deposited by electroplating (potassium gold cyanide-system, Aurall 292, Shipley Company) into the sidewall resist structures. The gold thickness was approximately 4–6  $\mu\text{m}$ . Fig. 7(b) depicts example of metallized electrodes over a 90° corner. Prior to patterning, the substrates were sputtered with a 50-nm-thick gold seed layer. After the electroplating, this seed layer was etched in cold 4 : 4 : 9 HCl : HNO<sub>3</sub> : H<sub>2</sub>O in order to isolate the structures.

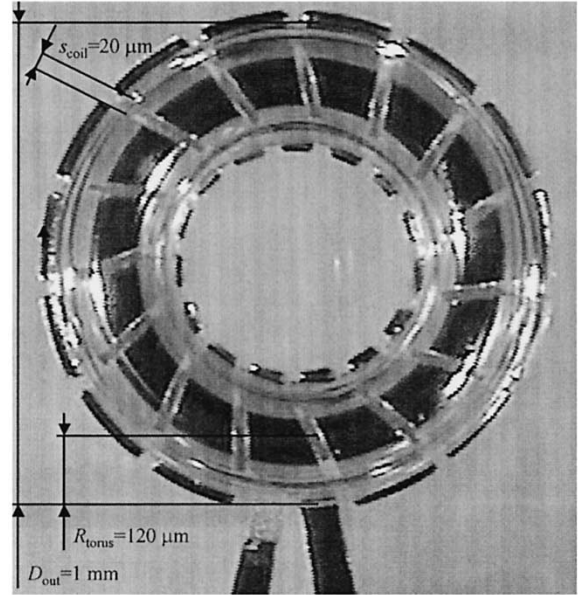
Four-point probe measurements were conducted on electroplated gold samples to measure the electrical resistivity. A constant current was applied and the voltage was recorded with a cryostat system (Maglab 2000, Oxford Instruments, Eynsham, U.K.). Thickness measurements were performed using a mechanical stylus profilometer (Alpha-Step 200, KLA Tencor, San Jose, CA). The electrical resistivity was found to be  $2.60 \cdot 10^{-8} \Omega \cdot \text{m}$ , which is close to the tabulated value for bulk gold [23],  $2.20 \cdot 10^{-8} \Omega \cdot \text{m}$ .

#### F. Assembly of Inductor

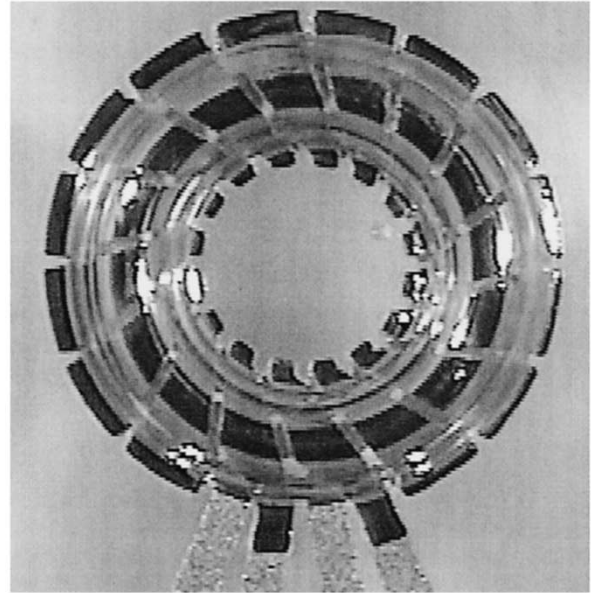
In order to obtain a complete functional inductor, two metallized substrates have to be bonded. This was achieved by thermo compression (at 75-bar pressure) with a heat-curing adhesive (EpoTek OG198-50, Epoxy Technology, Billerica, MA, cured at 120 °C for 15 min). The aim is to achieve a low contact resistance by ensuring a proper metal–metal contact at the gold interfaces. The inductor will exhibit a serial resistance containing contributions from both contact points, as well as intrinsic material properties of the electroplated gold. The contact resistance is also affected by alignment errors. Fig. 8 shows an example of an assembled inductor and an 8 : 8 coreless transformer.

### IV. RESULTS

The components were measured using a Rohde & Schwarz ZVC network analyzer and a Karl Süss PA200 probe station. The two-port  $S$ -parameters were measured on-chip with the RF probes over a frequency range from 10 MHz to 8 GHz. During the measurements, the polymer chip containing the coil was resting on the metallic measurement chuck. A set of unconnected pads was measured to determine the parasitics. The parasitics from the unconnected pads were deembedded from the



(a)



(b)

Fig. 8. Light optical microscope photograph of: (a) an assembled inductor and (b) an 8 : 8 coreless transformer.

measurement data by subtracting the  $Y$ -parameters of the unconnected pads from the  $Y$ -parameters of the inductor and converting the results back to  $S$ -parameters. In addition, the leads joining the pads to the component were measured. The inductance from the leads ( $2 \cdot L_{\text{lead}}$ ) was 0.56 nH.

The dimensions of the measured components were  $r_{\text{torus}} = 120 \mu\text{m}$ ,  $D_{\text{out}} = 1 \text{ mm}$ ,  $s_{\text{coil}} = 20 \mu\text{m}$ , metal thickness 4  $\mu\text{m}$ , and the number of turns 15. Fig. 9 shows the results, when the equivalent circuit presented in Fig. 4 is fitted to the measured  $S$ -parameters. The series resistance in the fitted equivalent circuit behaves according to (11). The coefficient  $\alpha_1 + \alpha_2$  used in (11) is 0.8. The coefficient value is in good agreement with previous results [24], [25]. The fitted equivalent-circuit parameters are shown in Table I. For comparison, Table I also shows ana-

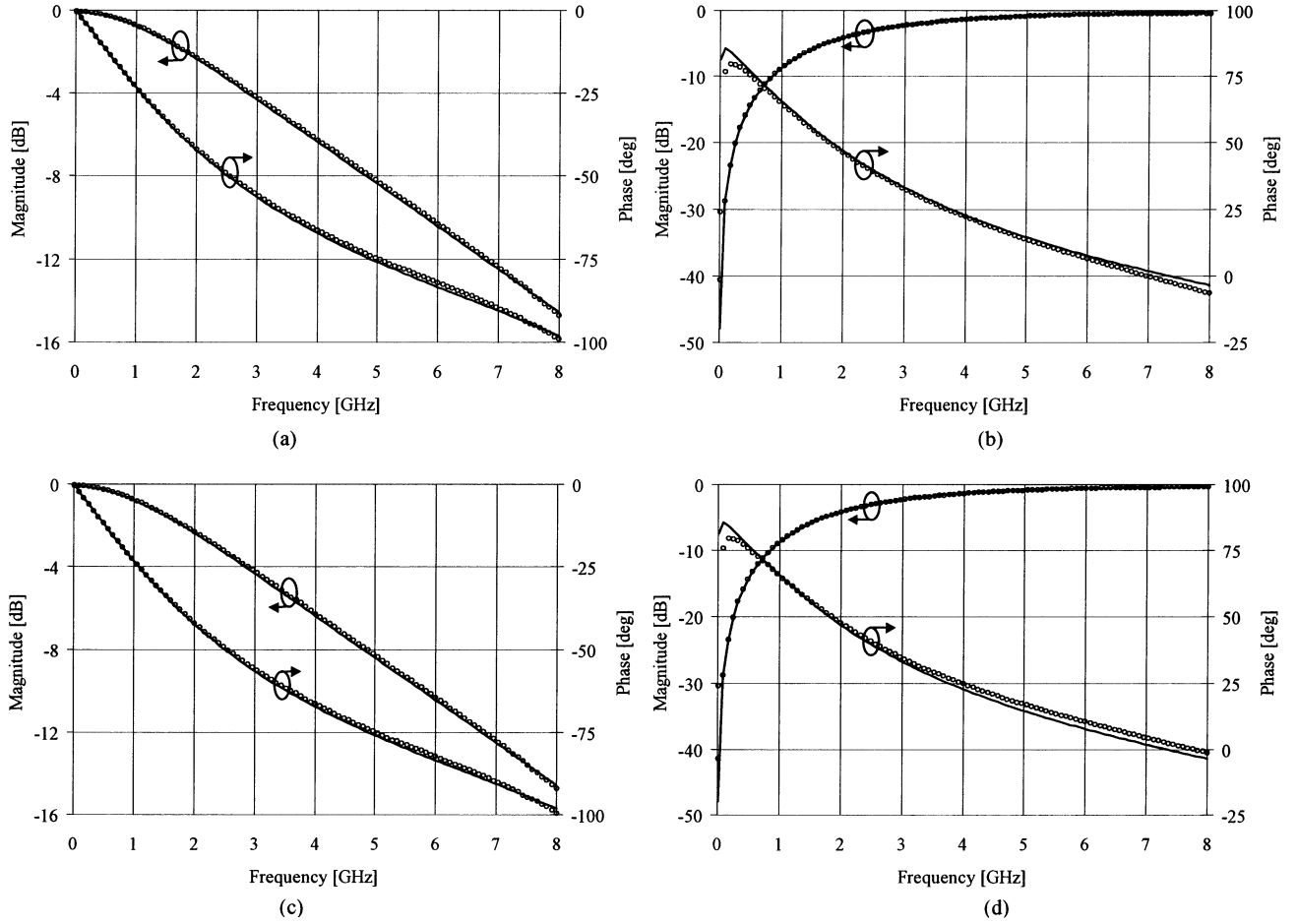


Fig. 9. Diagrams show measured (points) and simulated (solid lines) magnitude and phase versus frequency for: (a)  $S_{21}$ -parameters, (b)  $S_{11}$ -parameters, (c)  $S_{12}$ -parameters, and (d)  $S_{22}$ -parameters.

TABLE I  
EQUIVALENT-CIRCUIT MODEL PARAMETERS

| Parameters    | Analytically<br>calculated values | Fitted to measured S-<br>parameters |
|---------------|-----------------------------------|-------------------------------------|
| $f_{cr}$      | -                                 | 700 MHz                             |
| $R_{turn}$    | 30 m $\Omega$                     | 32 m $\Omega$                       |
| $R_{ground1}$ | -                                 | 80 k $\Omega$                       |
| $R_{ground2}$ | -                                 | 21 $\Omega$                         |
| $L_{turn}$    | 0.357 nH                          | 0.4 nH                              |
| $C_{turn1}$   | 32 fF                             | 35 fF                               |
| $C_p$         | 32 fF                             | 40 fF                               |
| $C_{ground}$  | 8 fF                              | 6.2 fF                              |

lytical values for the equivalent circuit that are calculated from (11)–(15).

To calculate  $Q$  and  $L$ , the inductor impedance must be calculated from the measured  $S$ -parameters. Fig. 10 shows measured and simulated real and imaginary parts of the inductor impedance as a function of frequency. These are calculated according to (2) and (3) for T- and  $\pi$ -networks, respectively. From the imaginary part of the impedance, the inductance of the coil is calculated to be 6.61 nH at 1 GHz, including the leads.

It was stated in Section II that the calculation of the inductor impedance using T- and  $\pi$ -networks neglects some parasitic

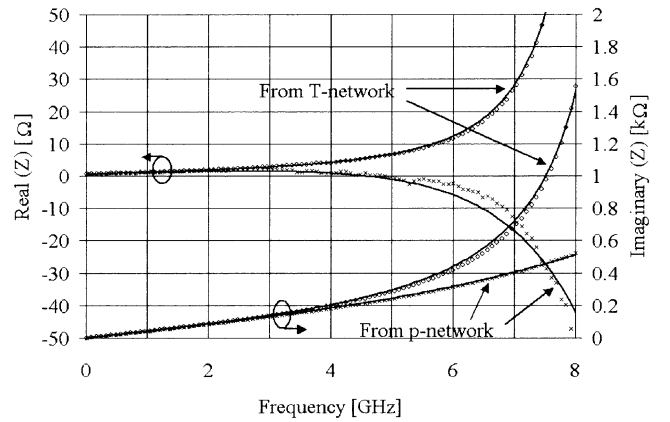


Fig. 10. Measured (points) and simulated (solid lines) imaginary and real parts of the impedance ( $Z$ ) of the toroidal inductor as a function of frequency. The  $Z$  is calculated from measured and simulated  $S$ -parameters using both T- and  $\pi$ -network configurations.

losses. In addition, if the equivalent circuit needed for the inductor modeling is more complicated than the T- or  $\pi$ -network, the behavior of the impedance can be unpredictable. For instance, Fig. 10 shows that the parasitic capacitance to ground  $C_{ground}$  and substrate losses  $R_{ground1}$  are important. The  $Y_1$  of the  $\pi$ -network does not include this kind of behavior. This makes the real part of the impedance calculated using the  $\pi$ -network negative. Therefore, the T-network model is selected to

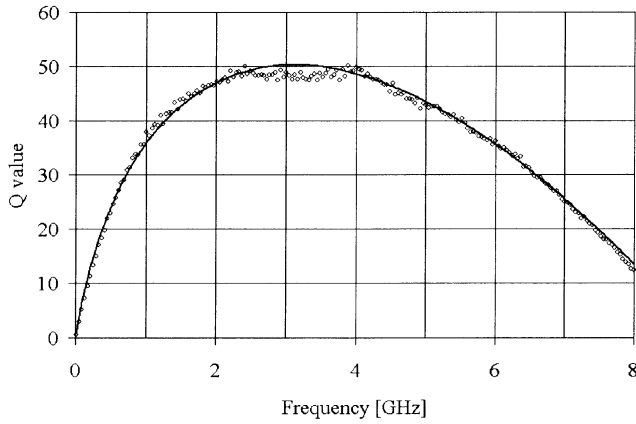


Fig. 11. Measured (points) and simulated (solid line)  $Q$  of the toroidal inductor as a function of frequency.

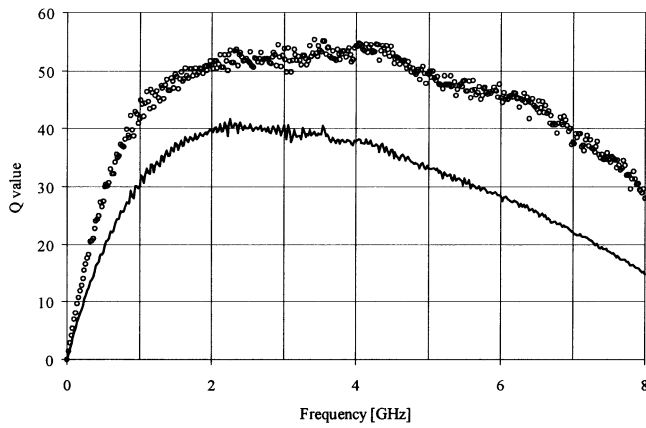


Fig. 12. Measured temperature dependency of the  $Q$  as a function of frequency. The solid line is measured  $Q$  at 110 °C and the points are measured  $Q$  at -25 °C.

represent the inductor and (2) is used to calculate the impedance of the inductor. Fig. 11 shows measured results and simulated  $Q$  of the inductor.

The effect of temperature on the inductor performance was studied. The inductor  $S$ -parameters were measured over the temperature range -25 °C to 110 °C. Results show that the inductance value has a small temperature dependency of 30 ppm/K. Temperature dependence is due to geometrical changes that are caused by the thermal expansion and contraction of the polymer substrate and the metal electrodes. Fig. 12 shows the temperature dependence of the inductor  $Q$ . Analysis of the measurement results showed that the changes are mainly due to the real part of the impedance. This means that the change of the  $Q$  is caused by the temperature dependence of metal conductivity.

One of the advantages of the toroidal coil is that the electromagnetic field is mostly contained inside the coil. However, some of the field still leaks outside the toroid and, thus, the substrate has an effect on the  $Q$  behavior. Fig. 13 compares the  $Q$  behavior between PC and COP substrates. The lower  $Q$  after 4 GHz in the PC substrate is due to the higher substrate losses.

Measurements show that the dc current handling capacity of the coil is 0.3 A. The current handling capacity of the toroidal inductor is limited at the moment by the polymer substrate. The polymer substrate cannot stand temperatures over 150 °C. When current flows in the coil, the resistive loss heats the substrate.

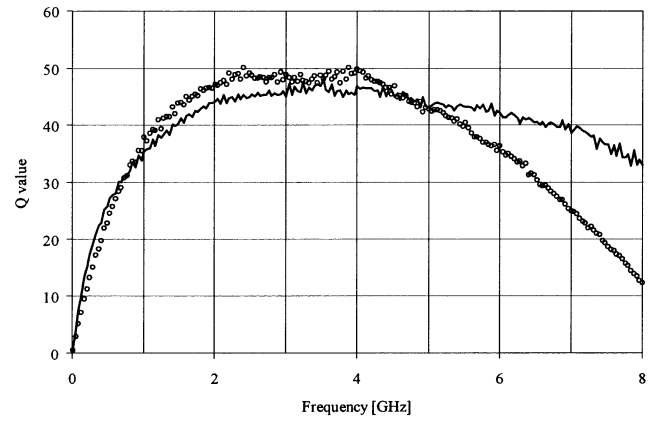


Fig. 13. Effect of the substrate on the  $Q$  of the inductor as a function of frequency. The solid line is the measured  $Q$  of an inductor ( $L = 5.63$  nH) on the COP substrate (loss tangent = 0.0002 and  $\epsilon = 2.3$  at 1 MHz). The points are the measured  $Q$  of an inductor ( $L = 6.61$  nH) on the PC substrate (loss tangent = 0.01 and  $\epsilon = 3.5$  at 1 MHz).

The thermal conductance of the polymer defines how well this heat is dissipated.

It should be pointed out that the manufacturing technology presented here is not limited to RF inductors. It can be adapted, for example, for fabrication of RF transformers. A fabricated test structure to evaluate a 3-D coreless transformer with turn ratio 8:8 is shown in Fig. 8(b).

The comparison of the measured and simulated  $S_{21}$  for a coreless transformer with an 8:8 turn ratio is depicted in Fig. 14. The dimensions of the transformer under the test are: 1) outer diameter of the coil, 1 mm; 2) radius of the cross section of a coil turn, 120  $\mu\text{m}$ ; 3) thickness of the gold, 5  $\mu\text{m}$ ; 4) separation between the turns, 20  $\mu\text{m}$ ; and 5) thickness of the polymer substrate, 1.2 mm. Agilent HFSS was used as a simulation tool. Measured and simulated insertion losses are -12.1 and -6.5 dB at 1 GHz, respectively. The large discrepancy between simulated and measured results is due to the model limitations. Since the ratio between the size of the coil and thickness of the metal is large, the model cannot take into account the thickness of the metal. As a result, current crowding effects are not included in the model. The observed high insertion loss is due to large electromagnetic field leakage. This leads to weak coupling between the transformer primary and secondary windings.

The use of a ferrite core is a traditional way to improve coupling between primary and secondary windings of transformers. Fig. 14 shows simulated  $S_{21}$  behavior for an 8:8 transformer containing a ferrite core with a magnetic permeability of 15. It can be seen from this simulation that the insertion loss of the transformer could be reduced considerably.

## V. SUMMARY AND DISCUSSION

The possibility to manufacture truly 3-D toroidal structures in metal has been shown. There are several advantages of using microreplication technology, which are: 1) truly 3-D structures can be integrated in a chip scale package of an RF IC; 2) it is possible to integrate arrays of components at the wafer level, while packaging of the MEMS component takes place at wafer level; 3) clearly higher quality factors compared to planar coils are possible; 4) there is low interference with the surrounding circuits because most of the electromagnetic field is concentrated



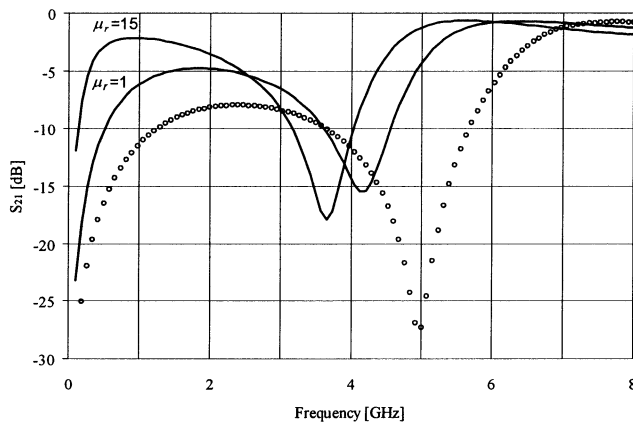


Fig. 14. Measured (points) and simulated (solid lines)  $S_{21}$ -parameters as function of frequency for 8:8 coreless transformer ( $\mu_r = 1$ ) and for transformer with ferrite core ( $\mu_r = 15$ ).

inside the torus; and 5) the fabrication technique is well suited for high-volume manufacturing.

The reported manufacturing technique can also be extended to become a flexible packaging platform. By embedding different components (not only inductors) in the polymer substrate and surface-mounted discrete circuits or ICs, a flexible and multifunctional packaging platform is created, i.e., it enables a low-cost system-in-a-package approach.

The main drawback with the current solution is that the polymers used are not compatible with the temperature cycle in soldering reflow processes. There are, however, polymers available that exhibit both low dielectric constant and high heat resistance. Future research will address these kinds of materials.

There is also the issue of environmental testing. Initial tests in humidity chambers and with thermal cycling looks promising. However, more work needs to be done in this area. Specifically, properties like thermal conductivity and expansion have to be carefully analyzed.

#### ACKNOWLEDGMENT

The authors acknowledge the participation of H.-O. Scheck, Nokia, Helsinki, Finland, O. Öhman, Åmic AB, Uppsala, Sweden, P. Siukonen, Nokia, and M. Andersson, Nokia. The authors further acknowledge V. Hurskainen, Nokia, for making the HFSS simulation.

#### REFERENCES

- [1] N. M. Nguyen and R. G. Meyer, "Si IC-compatible inductors and LC-passive filters," *IEEE J. Solid-State Circuits*, vol. 25, pp. 1028–1031, Aug. 1990.
- [2] J. N. Burghartz, D. C. Edelstein, M. Soyuer, H. A. Ainspan, and K. A. Jenkins, "RF circuit design aspects of spiral inductors on silicon," *IEEE J. Solid-State Circuits*, vol. 33, pp. 2028–2034, Dec. 1998.
- [3] *Product Catalog for RF Inductors*, Coilcraft Inc., Cary, IL. [Online]. Available: [http://www.coilcraft.com/prod\\_rf.cfm](http://www.coilcraft.com/prod_rf.cfm).
- [4] K. B. Ashby, I. A. Koullians, W. C. Finley, J. J. Bastek, and S. Moinian, "High  $Q$  inductors for wireless applications in a complementary silicon bipolar process," *IEEE J. Solid-State Circuits*, vol. 31, pp. 4–9, Jan. 1996.
- [5] J. N. Burghartz, D. C. Edelstein, K. A. Jenkins, and M. D. Hulvey, "High- $Q$  inductors in standard silicon interconnect technology and its application to an integrated RF power amplifier," in *Int. Electron Devices Meeting Tech. Dig.*, Dec. 1995, pp. 1015–1017.
- [6] C. P. Yue and S. S. Wong, "On-chip spiral inductors with patterned ground shields for Si-based RF ICs," *IEEE J. Solid-State Circuits*, vol. 33, pp. 743–752, May 1998.

- [7] J. N. Burghartz, D. C. Edelstein, K. A. Jenkins, and M. D. Hulvey, "Microwave inductors and capacitors in standard multilevel interconnect silicon technology," *IEEE Trans. Microwave Theory Tech.*, vol. 44, pp. 100–104, Jan. 1996.
- [8] J. Y.-C. Chang, A. A. Abidi, and M. Gaitan, "Large suspended inductors on silicon and their use in a 2  $\mu$ m CMOS RF amplifier," *IEEE Electron Device Lett.*, vol. 14, pp. 246–248, May 1993.
- [9] J. Y. Park and M. G. Allen, "Packaging-compatible high  $Q$  microinductors and microfilters for wireless applications," *IEEE Trans. Adv. Packag.*, vol. 22, pp. 207–213, May 1999.
- [10] D. J. Young, V. Malba, J.-J. Ou, A. F. Bernhards, and B. E. Boser, "Monolithic high-performance three-dimensional coil inductors for wireless communication applications," in *Int. Electron Devices Meeting Tech. Dig.*, Dec. 1997, pp. 67–70.
- [11] N. Chomnawang and J.-B. Lee, "On-chip 3D air core micro-inductor for high-frequency applications using deformation of sacrificial polymer," *Proc. SPIE*, vol. 4334, pp. 54–62, 2001.
- [12] G. W. Dahmann and E. M. Yeatman, "Microwave characteristics of meander inductors fabricated by 3D self-assembly," in *IEEE Electron Devices Meeting Conf.*, Nov. 13–14, 2000, pp. 128–133.
- [13] J. B. Yoon, B. K. Kim, C. H. Han, E. Yoon, and C. K. Kim, "Surface micromachined solenoid on-Si and on-glass inductors for RF applications," *IEEE Electron Device Lett.*, vol. 20, pp. 487–489, Sept. 1999.
- [14] F. W. Grover, *Inductance Calculations*. New York: Dover, 1973.
- [15] A. M. Niknejad and R. G. Meyer, "Analysis, design and optimization of spiral inductors and transformers for Si RF ICs," *IEEE J. Solid-State Circuits*, vol. 33, pp. 1470–1481, Oct. 1998.
- [16] H. Lakdawala, X. Zhu, H. Luo, S. Santhanam, L. R. Carley, and G. K. Fedder, "Micromachined high  $Q$  inductors in a 0.18- $\mu$ m copper interconnect low- $K$  dielectric CMOS process," *IEEE J. Solid-State Circuits*, vol. 37, pp. 394–403, Mar. 2002.
- [17] "Optimising planar inductors," VTT Automation, Helsinki, Finland, Res. Notes 2017, 2000.
- [18] R. Rhea, "Filters and oscillator using a new solenoid model," in *Appl. Microwave Wireless*, 2000, pp. 30–42.
- [19] O. Öhman, H. Sjödin, B. Ekström, and G. Jacobsson, "Microfluidic structure and process for its manufacture," Pharmacia Biosensor, Uppsala, Sweden, Int. Publication WO 91/16 966, Dec. 27, 1994.
- [20] —, "Microfluidic structure and process for its manufacture," U.S. Patent 5 376 252, Dec. 27, 1994.
- [21] O. Rötting, W. Röpke, H. Becker, and C. Gärtner, "Polymer microfabrication technologies," *Microsyst. Technol.*, vol. 8, pp. 32–36, 2002.
- [22] C.-H. Han and E.-S. Kim, "Study of self-limiting etching behavior in wet isotropic etching of silicon," *Jpn. J. Appl. Phys.*, vol. 37, pp. 6939–6941, 1998.
- [23] G. T. Meaden, *Electrical Resistance of Metals*. New York: Plenum, 1965, p. 1.
- [24] B. L. Ooin, D.-X. Xu, P.-S. Kooi, and F.-J. Lin, "An improved prediction of series resistance in spiral inductor modeling with eddy-current effect," *IEEE Trans. Microwave Theory Tech.*, vol. 50, pp. 2202–2206, Sept. 2002.
- [25] V. Ermolov, H. Nieminen, K. Nybergh, T. Ryhänen, and S. Silanto, "Microsystem technologies for mobile communication products," *Surface Mount Technol. Int.* 2001, pp. 710–717, 2001.



**Vladimir Ermolov** received the M.Sc. and Ph.D. degrees from the Moscow Engineering Physics University (MEPhI), Moscow, Russia, in 1981 and 1986, respectively, both in engineering physics.

From 1981 to 1998, he was a Senior Research Associate with the Laboratory of Dielectric Devices, MEPhI, during which time he was a Visiting Researcher numerous times with the Department of Physics, Helsinki University, Helsinki, Finland, and the Fraunhofer Institute of Nondestructive Testing, Saarbrücken, Germany. In 1998, he joined the Nokia Research Center, Helsinki, Finland, as a Senior Research Engineer, where he has been a Project Manager for several MEMS projects. During his professional career, he has been involved in the areas of sensors for measurements of ocean parameters, acoustic devices for signal processing, surface acoustic wave (SAW) devices, variable acoustic devices, acoustic effects in magnetic materials and their technical applications, nonlinear effects in solid-state acoustical and nondestructive evaluation, and MEMS. He has authored and coauthored 47 scientific publications. He holds and co-holds 22 patents.

**Tomas Lindström** received the M.Sc. degree in engineering physics and Ph.D. degree in solid-state physics from Uppsala University, Uppsala, Sweden, in 1992 and 2000, respectively. His thesis concerned spectroscopic light scattering measurements on thin films and roughness growth.

From 1992 to 1995, he was with Sandvik Coromant, Sandviken, Sweden, where he was involved with metal-cutting technology. He is currently with Åmic AB, Uppsala, Sweden, where he is involved with lab-on-a-chip technologies for the biotechnical industry. His research interest includes metallization on polymers.



**Heikki Nieminen** received the Master of Science (Tech.) degree in engineering physics from the Helsinki University of Technology (HUT), Espoo, Finland, in 1999, and is currently working toward the Doctor of Science (Tech.) degree at HUT.

He is currently a Research Engineer with the Nokia Research Center, Helsinki, Finland. His research interests are focused on the design of microelectromechanical devices and reconfigurable RF circuits. He holds one patent.

**Mikael Olsson** received the M.Sc. degree in engineering physics from Uppsala University, Uppsala, Sweden, in 2000.

He is currently with Åmic AB, Uppsala, Sweden, where he is involved with lab-on-a-chip technologies for the biotechnical industry. His research interest includes microstructuring polymers.

**Michael Read** received the B.Sc. degree in industrial chemistry from the University of Wales, Wales, U.K., in 1985, and the Ph.D. degree in inorganic chemistry from the Royal Institute of Technology, Stockholm, Sweden, in 1991.

He was involved with process engineering and development with Pilkington Glass, Ericsson, and Toolex Alpha, where he was Technical Manager. He is currently Vice President of Marketing and Applications with Åmic AB, Uppsala, Sweden.

**Tapani Ryhänen** was born in Helsinki, Finland, on July 7, 1959. He received the Master of Science (Tech.) degree in engineering physics and Doctor of Science (Tech.) degree in applied electronics from the Helsinki University of Technology (HUT), Espoo, Finland, in 1986 and 1992, respectively.

From 1992 to 1995, he was with Vaisala Technologies Inc., where he designed micromechanical pressure and angular rate sensors. In February 1995, he joined Nokia Telecommunications, where he was a Research and Development Manager and a Senior Product Manager. In December 1998, he joined the Nokia Research Center, Helsinki, Finland, as a Principal Scientist, where he was responsible for the MEMS research program. Since April 2000, he has headed the Microsystem Technologies Group as a Senior Research Manager. He has authored or coauthored several publications on the theory, design, and characterization of ultra-low-noise superconducting thin-film magnetometers and microelectromechanical sensors, actuators, and systems. He holds six patents with several pending, which are related to micromechanical devices and systems. His current research focus is in the fields of RF MEMS, sensors, and integration of microsystems into portable electronics.

**Samuli Silanto**, photograph and biography not available at time of publication.

**Simon Uhrberg** received the B.Sc. degree in mechanical engineering from Uppsala University, Uppsala, Sweden, in 1998.

He was a mechanical consultant prior to joining Åmic AB, Uppsala, Sweden, in late 1998. He is currently involved with design and application development of polymeric biochips.